Journal of the Iranian Chemical Society (2022) 19:1319–1328
https://doi.org/10.1007/s13738-021-02380-z

ORIGINAL PAPER

Mechanistic insights of the adsorption of Eriochrome Black T by the formulated Mg–Al LDH-graphene oxide composite

Loknath Dhar[1] · Md Sajjadur Rahman[2] · Saddam Hossain[1] · Shamshad B. Quraishi[3] · Koushik Saha[1] · Farzana Rahman[4] · Uttam Kumar Sarker[5] · Mir Tamzid Rahman[1]

Received: 9 April 2021 / Accepted: 17 August 2021 / Published online: 26 August 2021

Abstract
Adsorption is one of the best techniques to mitigate industrial dye pollution. In this study, surface of the Mg–Al layered double hydroxide (LDH) was modified with graphene oxide (GO) to improve its adsorption efficacy of Eriochrome Black T (EBT) dye molecules. A higher correlation coefficient value of the Langmuir adsorption model indicated monolayer adsorption of EBT at the active sites of Mg–Al LDH. The optimum adsorption potential was obtained around 0.4 and 1.4 mmol of EBT per g of the LDH and the modified LDH, respectively, and both adsorbents followed pseudo-second-order kinetics. Molecular dynamics study revealed that both GO and LDH contribute to adsorb EBT. Hydrogen bonds, such as C-H…O, O–H…N, O–H…O = S, O–H…N, and N = O…H–O-Al are the major contributing forces behind the adsorption. Besides, π… alkyl, Mg…O = S, π…cation, π…anion, π…donor, π…sigma, and π…lone pair of interactions are the additional contributing forces behind the enhancement of the efficacy of the modified composite.

Keywords LDH · GO composite · Eriochrome Black T · Adsorption · Kinetics · Mechanism

Introduction

In modern days, people demand colorful, elegant, and gorgeous products. With the rapid increase of the world population, the demand for such products has been growing day by day. To meet the demand, the use of dye chemicals has been increased tremendously by the industries, including textile, paper, leather, printing, plastic, and carpet [1]. About 10,000 types of textile dyes are commercially available worldwide, and their production has been reached approximately 7.10×10^5 metric tons every year [2, 3]. After their use, they have been discarded into the water body directly or after treatment. Especially, dye-enriched textile effluents are not treated at the expected level in the industries of many developing countries, as they do not have the ability to invest in such expensive treatment plants. Thus, they sometimes dump the dye effluents directly into local water bodies, which leads to destroy the aquatic lives. The untreated colorful textile effluents are carcinogenic and mutagenic [4–6]. In order to minimize their harmful effects, many physical, chemical, and biological methods have been developed to remove the dyes from wastewater, such as membrane separation, flocculation, coagulation, adsorption, ozonization, aerobic, and anaerobic treatments [7]. Due to low cost, simplicity, high efficiency, selectivity, greenness, and wide-ranging availability, adsorption has been proved to be one of the most promising techniques for the extraction of dye molecules from wastewater [8, 9].

Layered double hydroxides (LDHs), also known as anionic clays, exhibit excellent properties, such as anion adsorptive, electroactive solids, heterogeneous catalysts, supercapacitors, and hybrid intercalation compounds [10–13]. These crystalline compounds are derived from the mineral hydrotalcite [14]. LDHs have been recognized as an effective adsorbent in the treatment of water [15]. It is a versatile

✉ Mir Tamzid Rahman
tamzidjuchem@gmail.com

1 Department of Chemistry, Jahangirnagar University, Savar, Dhaka 1342, Bangladesh

2 Department of Chemistry and Biochemistry, South Dakota State University, Brookings, SD 57007, USA

3 Chemistry Division, Atomic Energy Center, Bangladesh Atomic Energy Commission, Dhaka, Bangladesh

4 Department of General Educational Development, Daffodil International University, Dhaka, Bangladesh

5 Department of Chemistry, Hajee Mohammad Danesh Science and Technology University, Dinajpur, Bangladesh

class of two-dimensional (2D) ionic lamellar compounds. Due to the availabilities of a wide range of its composition and preparation variables, they are considered as a highly tunable brucite structure [16, 17]. To maintain its charge neutrality, the nanostructured materials contain positively charged metal hydroxide layers with intercalated exchangeable anions. LDH is symbolically represented by $[M^{2+}_{(1-X)} M^{3+}_{(X)} (OH)_2]^{X+} (A^{n-})_{X/} n\ mH_2O$, where $M^{2+}$is a divalent metal cation (e.g., Mg^{2+}, Mn^{2+}, Ni^{2+}, Zn^{2+}, Co^{2+}, Fe^{2+}, and Cu^{2+}) and M^{3+} is a trivalent metal cation (e.g., Al^{3+}, Fe^{3+}, Co^{3+}, Ni^{3+}, Mn^{3+}, and Cr^{3+}). The replaceable interlayer anions (A^{n-}) could be NO_3^-, Cl^-, CO_3^{2-}, and the water molecules are generally embedded among the hydroxide layers during the synthesis process [18–20]. Several methods are commonly used for preparing LDH, such as coprecipitation, ion exchange, rehydration, hydrothermal, secondary intercalation, and re-coprecipitation [21]. In this study, Mg–Al LDH was prepared by the coprecipitation technique as it is a greener technique [22].

Carbon-based materials, such as graphene and graphene oxide (GO) have been widely used for the dye removal process [23]. Graphene consists of single-layered carbon atoms that are tightly packed in a two-dimensional honeycomb-like structure [24, 25]. Graphite is the basic material for preparation of individual graphene or GO nanosheets. GO is a resource of great interest in the adsorption-based technologies because of its large surface area, π-electron containing surface, and functionalities, such as hydroxyl, carboxylic, carbonyl, and epoxide groups of the surface, and its high water solubility [26, 27]. In this experiment, the surface of LDH was modified with GO in a shielding manner to enhance its adsorption potentiality for the anionic species. The synergistic action of both LDH and GO in the nanocomposites will improve their adsorption ability [28].

The co-precipitation method was used to prepare the modified LDH. Eriochrome Black T was used as a model anionic dye to determine the efficacy of the modified LDH-GO. It is expected that the π-π stacking and hydrogen bonding interaction among the Eriochrome Black T and GO [29] might enhance the adsorption capability of modified LDH-GO.

Comparative experimental adsorption isotherm and kinetics studies [30, 31] on the adsorption reactions of the pure materials and the composite could prove the enhancement of the adsorption efficacy of the newly formed composite material for the Eriochrome Black T (EBT) dye molecules. However, it cannot be possible to understand the proper mechanism and the driving forces behind the enhancement of the efficacy. Simulating the adsorption reactions employing molecular dynamics (MD) technique could be an excellent alternative technique to the common experimental tools (e.g., NMR, FTIR, and XPS) to reveal the insights and mechanisms behind the adsorption reactions [32, 33].

The objectives of this study were to find out (i) at what extent the efficacy of the adsorption could be enhanced when the GO is laminated on the surface of the LDH, (ii) are both the GO and LDH simultaneously contribute to the adsorption of an anionic dye, (iii) which layer is more dominant for the adsorption, (iv) exploring of all possible driving forces behind the adsorption. In brief, the aims of this work were to investigate the adsorption mechanism and the reasons behind the enhancement of the adsorption potentiality of the LDH-GO composite compared to the pure LDH.

Materials and methods

Preparation of modified Mg–Al LDH with GO

The modified Mg–Al LDH with graphene oxide was prepared with our previously developed co-precipitation technique [34]. In the first part of the preparation, Mg–Al LDH intercalated with NO_3^- with a 3:1 molar ratio of Mg^{2+}/Al^{3+} and the total $[Mg^{2+} + Al^{3+}] = 0.5$ M was prepared by dissolving a stoichiometric amount of $Mg(NO_3)_2.6H_2O$ and $Al(NO_3)_3.9H_2O$ in 250 mL of de-ionized water followed by adding in a container with 250 mL de-ionized water. The mixing was carried out using a digital electric mixer overhead stirrer. To maintain the pH of the reaction at 10–10.5, 1.5 M NaOH was used throughout the reaction. Nitrogen gas was used to degasify the solution mixture, which helped to prevent forming of CO_3^- ions. The resulting precipitate ('Mg–Al LDH or LDH cake') was separated from the suspension through filtration using a vacuum suction glass filtering filtration unit with a Buchner funnel. It was washed with distilled water carefully and thoroughly to neutralize the pH. The precipitate was dried in an oven for 30 h at 60 °C followed by the products were finely ground with a mortar and pestle.

Graphene oxide was prepared from graphite powder using modified Hummer's method. About 0.1 g of graphite powder, 2 g of $NaNO_3$, and 46 mL of concentrated H_2SO_4 were added and stirred vigorously using a magnetic stirrer for 3 h into 1000 ml beaker. The temperature was maintained at less than 10 °C using an ice bath and monitored by a glass laboratory thermometer. To oxidize the solution, 8 g of $KMnO_4$ was gradually added to the solution and stirred for 1 h at 35 °C. After that, 92 mL of distilled water was added and stirred the solution for another 15 min at 98 °C. In order to complete the oxidation process, 280 mL of distilled water and 40 ml of 30% H_2O_2 were added and stirred the solution for 1 h. Then the suspension was filtered, washed with acetone, dried at 30 °C, and grounded into a fine powder to obtain graphite oxide for further use.

Finally, 5 g of the LDH cake was added to 100 mL of degasified distilled water. The solution was refluxed for 24 h

at 100 °C followed by the solution was instantly transferred into an ultrasonic bath to sonicate it for 3 h, which is called delaminated of LDH. Meanwhile, 0.1 g of graphite oxide solution was prepared using the same amount of water and sonicated it for 1 h. Through this process, the graphite oxide was turned into graphene oxide. When both the solution temperatures reached the room temperature, GO solution was carefully added to the LDH solution and was stirred for 1.5 h at 250 rpm. Filtration was used to isolate the resulting precipitate, and it was washed 2–3 times with distilled water. The precipitate was dried at 60 °C for 24 h, and the final Mg–Al LDH/GO product was grounded into fine powder to use it for further wastewater treatment. The proof of its successful formation was submitted in our previously submitted manuscript [34].

Adsorption isotherms

To evaluate the adsorption isotherms, 50 mL of Eriochrome Black T (EBT) dye solutions of varying concentrations (0.01–1.8 mmol/L) were prepared in de-ionized water and 0.01 g of the adsorbents (pure LDH and LDH-GO) were taken and shaken for 24 h at 250 rpm to complete the adsorption at room temperature. Then UV–Visible spectrophotometer was used to examine the adsorption isotherms.

Kinetics of EBT removal

The kinetic study of EBT was conducted at three different temperatures (10, 30 and 60 °C) with the pure LDH and the modified LDH. In a three-neck round-bottom flask, 250 ml 2 mmol/L dye solution and 0.05 g of both the adsorbents were mixed with continuous stirring using a digital electric mixer overhead stirrer. The solution mixtures were collected at different time intervals of 5, 10, 15…120 min. Exactly 2 mL of solution was diluted to the range of 0–20 ppm range to prepare the standard solutions. Samples and standards mixture were analyzed employing UV spectrophotometer.

Molecular dynamics study

Graphene sheet was prepared using Nanotube Modeler, which helped to generate XYZ coordinates of the graphene sheet [35]. Gauss view 5.0.8 and Gaussian 09 software packages [36, 37] were used to transform the graphene sheet into targeted model graphene oxide (GO). Mg–Al layered double hydroxide (LDH) intercalated with NO_3^- layers were also drawn in between two GO layers, and the whole composite structure was optimized it at mechanics level of theory at gaseous phase. The three-dimensional structure of the Eriochrome Black T (EBT) was obtained from PubChem [38] and optimized it at same level of theory for further molecular dynamics study.

The molecular dynamic (MD) simulations were performed to investigate how the GO-LDH composite adsorbs EBT molecules. All the simulations were conducted at gas phase using YASARA dynamics tool [32, 39]. The detailed information about AMBER14 force field, periodic boundary condition, energy minimization, particle-mesh Ewald (PME) method, cut-off distance 8 Å, temperature, and pressure were set the same as in one of our previously published articles [33]. In this study, cell size was always kept 5 Å larger than the reactions, and multiple time-step algorithm was employed with time step 2.00 fs [40, 41]. All the simulations were performed for 5 ns, since their potential energies were stable. The adsorption reaction was simulated at both low- and high-density environments to figure out the mechanism behind it. Firstly, the reaction simulation was conducted in low-density (46.28 g/L) cell box to mimic a low concentration reaction environment, where the LDH-GO composite: EBT ratio was 1:100. After that, composite: EBT ratios of 1:25, 1:50, and 1:100 were simulated with the cell box densities of 156.94, 239.65, and 427.93 g/L, respectively to find out all possible adsorption sites of the model composite and to analyze the nonbonding interactions responsible to successfully adsorb the EBT molecules. Finally, all the simulation data and energy profiles were analyzed using the default analysis macro file of YASARA. Structural features, intermolecular interactions, bond types, and bond distances were analyzed using Discovery Studio Visualizer [42].

Results and discussion

Adsorption of EBT with LDH and LDH-GO

Since EBT is an anionic dye, LDH effectively removes them from the aqueous solution through anion exchange process. Modified LDH with GO removes the EBT not only by anion exchange but also by the surface adsorption on GO. Figure 1 shows the equilibrium adsorption isotherm of LDH and LDH-GO by varying the EBT concentration. As the equilibrium concentration was (C_e, mmol/L) increased, the amount of equilibrium adsorption (q_e, mmol/g) was also increased. The highest amount of equilibrium adsorptions (q_e) were obtained at around 0.4 and 1.4 mmol of EBT per g of LDH and modified LDH after attaining equilibrium (C_e) at 0.2 and 1.0 mmol/L, respectively. Such findings indicate that the adsorption potential of the modified composite increases over three times. In order to understand the reaction mechanism between the adsorbates and adsorbents, Langmuir and Freundlich adsorption isotherm models were analyzed [31]. The equations are following:

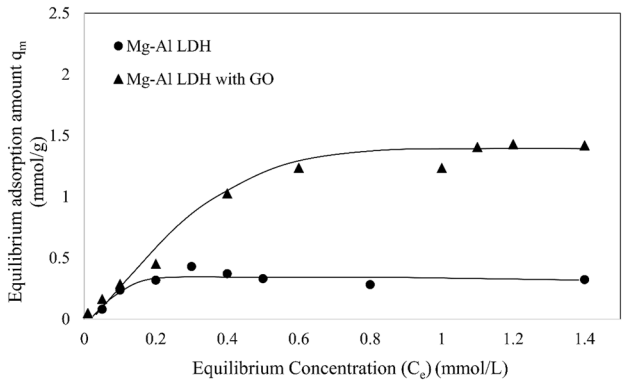

Fig. 1 Equilibrium adsorption isotherm of Mg–Al LDH and Mg–Al LDH with GO by varying initial EBT concentration

$$Langmuir: \frac{C_e}{q_e} = \frac{1}{b \cdot Q_0} + \frac{C_e}{Q_0} \quad (1)$$

$$Freundlich: \log q_e = \log k + \frac{1}{n} \log C_e \quad (2)$$

where C_e is the equilibrium concentration of adsorbate (mmol/L), q_e is the maximum amount of adsorption (mmol/g), Q_0 is the adsorbate concentration corresponding to monolayer coverage, b is the Langmuir constant (L/mmol), K and n are the Freundlich constants. The parameters of the Langmuir and Freundlich models for EBT adsorption by LDH and LDH-GO are listed in Table 1.

Langmuir adsorption model suggests a monolayer adsorption mechanism and no interaction among adsorbate molecules. On the contrary, Freundlich adsorption model describes a multilayer adsorption mechanism with intermolecular interaction among the adsorbates [30, 34]. In this study, higher correlation coefficients (R^2 values) were observed in Langmuir model than those of Freundlich model. Therefore, Langmuir model could describe the EBT adsorption better on the materials. It can be assumed from the outcomes of the models that the EBT molecules were adsorbed on the active sites of the adsorbent with no interaction among each other. Langmuir adsorption parameters Q_0 and b were calculated from the slope and intercept of the C_e/q_e versus C_e plot (Fig. 2a) and Freundlich adsorption parameters K and 1/n were calculated from the slope and intercept of the log q_e versus log C_e plot (Fig. 2b). The equilibrium parameter R_L was calculated using the following equation:

$$R_L = \frac{1}{1 + bC_0} \quad (3)$$

Table 1 Langmuir and Freundlich parameters for EBT removal by Mg–Al LDH and Mg–Al LDH with GO

Adsorbent	Langmuir model				Freundlich model		
	R^2	Q_0 (mmol/g)	b (L/mmol)	R_L	R^2	K	1/n
Mg–Al LDH	0.98	0.32	88.16	0.05	0.56	0.69	0.48
Mg–Al LDH with GO	0.97	1.60	7.17	0.12	0.94	1.62	0.53

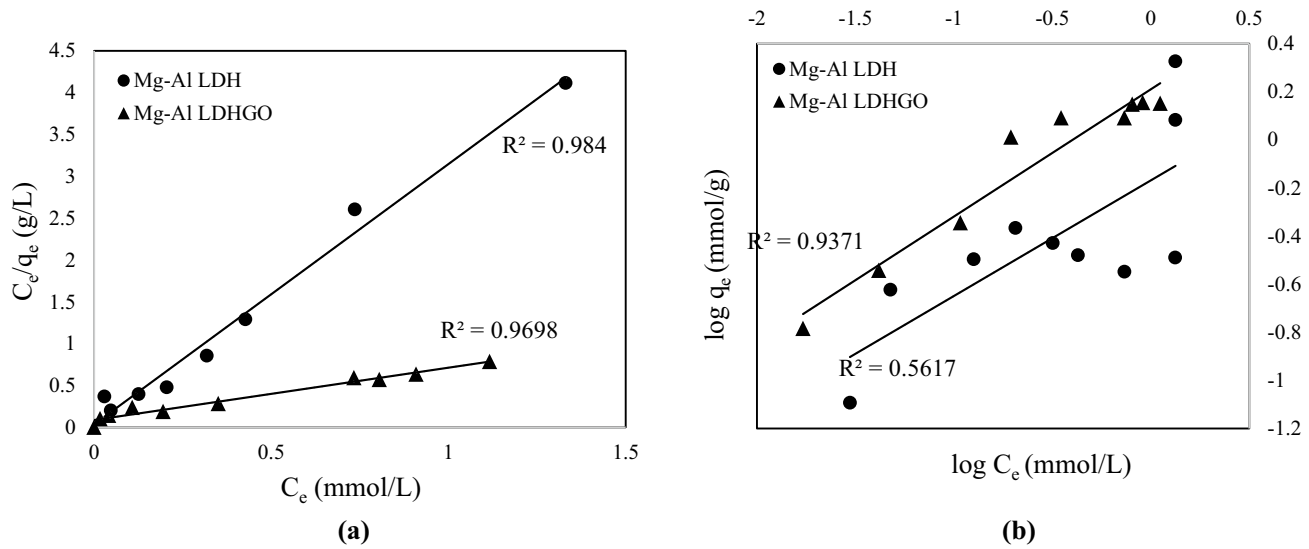

Fig. 2 Langmuir **a** and Freundlich **b** adsorption model for EBT adsorption on Mg–Al LDH and Mg–Al LDH with GO

where C_0 is the highest initial adsorbate concentration (mmol/L) and R_L values less than 1 shows the favorable adsorption of EBT on the active sites of adsorbents.

Kinetics of EBT removal through Mg–Al LDH and Mg–Al LDH/GO

To understand the adsorption mechanism and stability, kinetic studies were conducted at three different temperatures (e.g., 10, 30, and 60 °C) for 2 h. Figure 3a and b represents the removal percentage of EBT by Mg–Al LDH and Mg–Al LDH-GO, respectively. Figures show that the EBT adsorption patterns were quite similar for both adsorbents. At 10 °C, after obtaining the equilibrium point, the percentage of adsorption became stable with time. Lower temperature implies lower kinetic energy and lower entropy, whereas higher temperature refers to higher entropy [15]. Therefore, at 30 °C and 60 °C, the percentage of adsorption was increased first, but after saturation of the active sites percentage of adsorption tends to decreased and desorption started to occur for both adsorbents. But, the desorption rate was observed lower using Mg–Al LDH-GO composite in comparison with Mg–Al LDH. EBT is an anionic dye and tends to adsorb on Mg–Al LDH through anion exchange with NO_3^- ions. At higher temperature, there was a competition among the NO_3^- ions and EBT molecules to be held among the Mg–Al hydroxide layers due to comparable charge density. Therefore, the desorption occurred at elevated temperature and longer time of reaction. For the modified Mg–Al LDH-GO composite, the positive charged density of Mg–Al LDH surface gets decreased due to charge compensating with negatively charged oxygenic functional groups of GO. Therefore, attraction forces among the active sites of the Mg–Al LDH and EBT molecules became weak. It is assumed that there are some hydrogen bonding and some other nonbonding attraction might be the driving force of higher adsorption and lower desorption of EBT molecules on Mg–Al LDH-GO composite.

To get some ideas about the reaction mechanism of EBT adsorption by the LDH and LDH-GO, the pseudo-1st order and pseudo-2nd order kinetics studies were performed. Equation of Pseudo-1st order rate reaction is following below-[30, 31].

$$-\ln(1-x) = K_1 t \tag{4}$$

Here, x is the % of EBT removal, t is the time in min, and k_1 refers to the pseudo-1st order rate constant (min^{-1}).

Equation for the Pseudo-2nd order reaction is following-[30, 31]

$$\frac{1}{q_t} = \frac{1}{K_2 q_e^2} + \frac{t}{q_e} \tag{5}$$

Here q_t is the amount (mmol/g) of EBT removal at reaction time (min), q_e is the amount (mmol/g) of EBT removal at equilibrium, and k_2 is the pseudo-2nd order rate constant (g $mmol^{-1}$ min^{-1}).

For these two kinetic models, the correlation coefficients (R^2-values), rate constants, and other parameters were estimated and shown in Table 2. The values of the parameters and the lower correlation coefficient value indicated that pseudo-1st order reaction kinetics was not suitable to describe the reaction mechanism for both LDH and LDH-GO. However, the higher correlation coefficient value was obtained for pseudo-2nd order kinetics at all the temperatures for both materials. It suggests that the reaction rates depend on the concentration of adsorbents (LDH and LDH-GO) and dye EBT molecules in the aqueous solution, where there is an excess amount of water and no change is observed in quantity after the reactions. The pseudo-2nd order reaction isotherm of EBT removal by (a) Mg–Al LDHs and (b) Mg–Al LDH with GO at temperatures of 10, 30, and 60 °C are shown in Fig. 4.

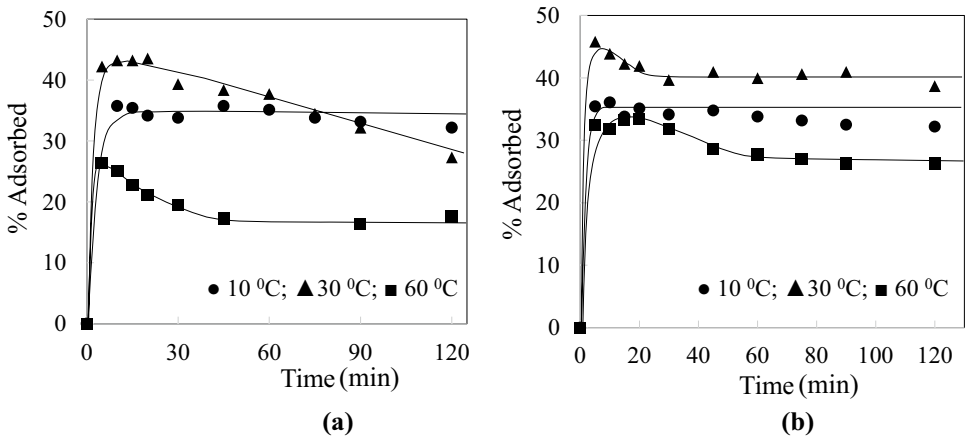

Fig. 3 The removal percentages of EBT by Mg–Al LDH **a** and modified Mg–Al LDH with GO **b** at 10, 30 and 60 °C

Table 2 Kinetic parameters for EBT removal by Mg–Al LDH and Mg–Al LDH with GO

Kinetics model	Adsorbent	Temperature (°C)	q_e (mmol/g)	R^2
Pseudo-1st order	Mg–Al LDH	10	3.7	0.06
		30	4.3	0.02
		60	2.7	4E-06
	Mg–Al LDH-GO	10	3.6	0.06
		30	4.6	0.07
		60	3.3	0.001
Pseudo-2nd order	Mg–Al LDH	10	3.26	1.00
		30	2.89	0.98
		60	1.76	0.98
	Mg–Al LDH-GO	10	3.23	1.0
		30	3.93	1.0
		60	2.60	1.0

Thermodynamic study of EBT removal by Mg–Al LDH and Mg–Al LDH/GO

The thermodynamic study was conducted at different temperatures such as 283, 303, and 333 K to determine the thermodynamic parameters (ΔG°, ΔH°, and ΔS°) using Eqs. (6) and (7) [28].

$$\Delta \dot{G} = -RT \ln Kc \tag{6}$$

$$\ln Kc = \frac{\Delta \dot{S}}{R} - \frac{\Delta \dot{H}}{RT} \tag{7}$$

where ΔG° is denoted for change in the standard Gibbs free energy (kJ/mol), ΔH° is denoted for change in the standard enthalpy (kJ/mol), ΔS° is denoted for change in the standard entropy (kJ/mol·K), R is the universal gas constant (8.316 J/mol K), and T is the absolute temperature (K).

The thermodynamic parameters are presented in Table 3. The negative values of ΔG° recommend that the adsorption of dye EBT molecules on the Mg–Al LDH and Mg–Al LDH-GO were spontaneous and practically possible. The negative values of ΔH° show that the adsorption of EBT molecules was exothermic in nature. The positive values of ΔS° suggest the high randomness of the solid/solution at the EBT molecules adsorption in an aqueous medium of Mg–Al LDH and Mg–Al LDH-GO.

Adsorption mechanism obtained from MD simulation

The composite comprises graphene oxide (GO)-Mg–Al layered double hydroxide (LDH) intercalated with NO_3^-, where both attractive and repulsive forces play the roles for the successful delamination and for the stability of the

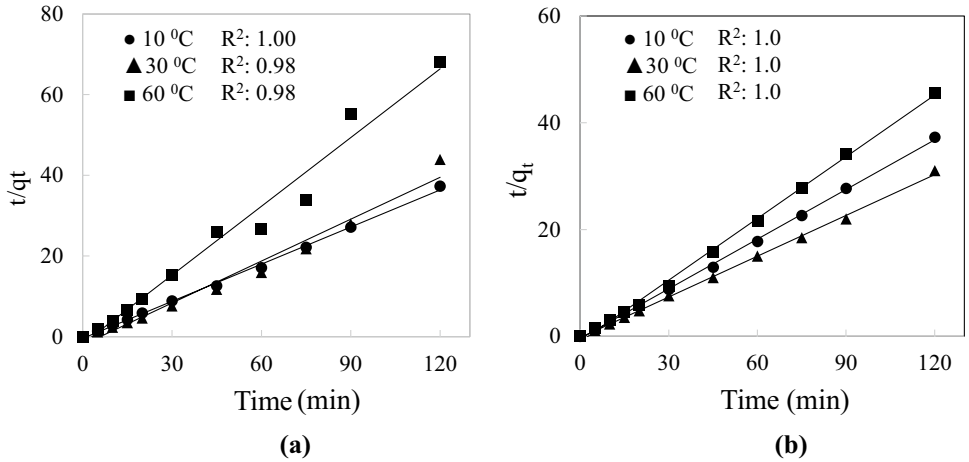

Fig. 4 Pseudo-2nd order reaction isotherm of EBT removal by Mg–Al LDH **a** and Mg–Al LDH with GO **b** at 10, 30, and 60 °C

Table 3 The thermodynamic parameters for EBT removal by Mg–Al LDH and MG–Al LDH with GO

Adsorbent	Thermodynamic parameters				
	ΔH° (kJ/mol)	ΔS° (kJ/mol.K)	ΔG° (kJ/mol)		
			283 K	303 K	333 K
Mg–Al LDH	− 16.29	0.009	− 18.39	− 18.29	− 16.19
Mg–Al LDH-GO	− 6.01	0.005	− 6.96	− 7.82	− 6.26

composite. Figure S1 demonstrates the network of intermolecular interactions that exists in the composite. The range of the classical and non-classical hydrogen bond distances is 2.50–3.06 Å. Figure S2 and S3 shows two other attractive interactions, which are charge-charge interactions and the attractive forces from metal acceptors with bond distance range of 1.98–5.56 Å. Besides, repulsive forces, such as steric bumps through LDH layers, positive-positive/negative-negative charge repulsion, acceptor-acceptor/donor-donor atom repulsions, and the repulsion from metal (Mg)-donor have been observed from Figure S4 through S7, respectively.

One molecule of LDH-GO composite and 100 molecules of EBT have been taken to simulate the adsorption reaction at low-density condition to mimic the way to adsorb EBT at low concentration environment. It helps to find out how an EBT approaches the composite, starts making interactions and gets stabilized on the surface of it. It is found that the GO layer attracts an EBT molecule from 0 ns (Fig. 5). After some time, the EBT molecule makes higher number of nonbonding interactions to a GO layer, and approaches towards the LDH layer at 2.5 ns. This molecule then makes nonbonding interactions with both GO and LDH layers at 5 ns, and gets more stabilized (Fig. 5). The figure shows that only one non-classical C-H…O (2.72 Å) hydrogen bond between the composite and the EBT at 0 ns, but at 2.5 and 5 ns the number of nonbonding interactions has been increased. At 2.5 ns, the EBT forms stronger classical hydrogen bonds (e.g., O–H…N, O–H…O = S, and O–H…O = S with bond distances 1.69 to 2.17 Å) with the GO layer. Eventually, at 5.0 ns, N = O of EBT forms one more strong interaction with the O–H-Aluminum of the LDH (2.28 Å).

All other adsorption sites and involved nonbonding forces for the adsorptions are also needed to be explored. Thus, three high-density simulations with 1:25, 1:50, and 1:100 (composite: EBT) ratios are simulated. In the case of 1:25 composite: EBT simulation, three stable adsorption sites are obtained. Along with the conventional hydrogen bonds (Fig. 6a), some other nonbonding interactions from the pi-electron of the benzene rings (e.g., pi…alkyl (3.68–5.47 Å), pi…cation (4.75–4.96 Å), pi-donor…H–O (2.73 Å)), and metal (Mg) acceptor…O = S (3.08 Å) of the EBT molecules have been observed. Similarly, 1:50 and 1:100 composite: EBT simulations show newer adsorption sites with new types of nonbonding interactions, such as pi…lone pair (2.84 Å), pi…sigma (2.62 Å), and pi…anion (4.07 Å) (Fig. 6b and c). MD studies also proved that the adsorption reactions follow the Langmuir adsorption isotherm. However, at the supersaturation point, the intermolecular interactions e.g., pi…sulfur (5.17–5.26 Å) and pi…pi T-shaped (4.86–5.64 Å) among the EBT molecules could be observed (Fig. 6c).

Therefore, EBT molecules typically interact with the composite using hydrogen bond donor–acceptor atoms.

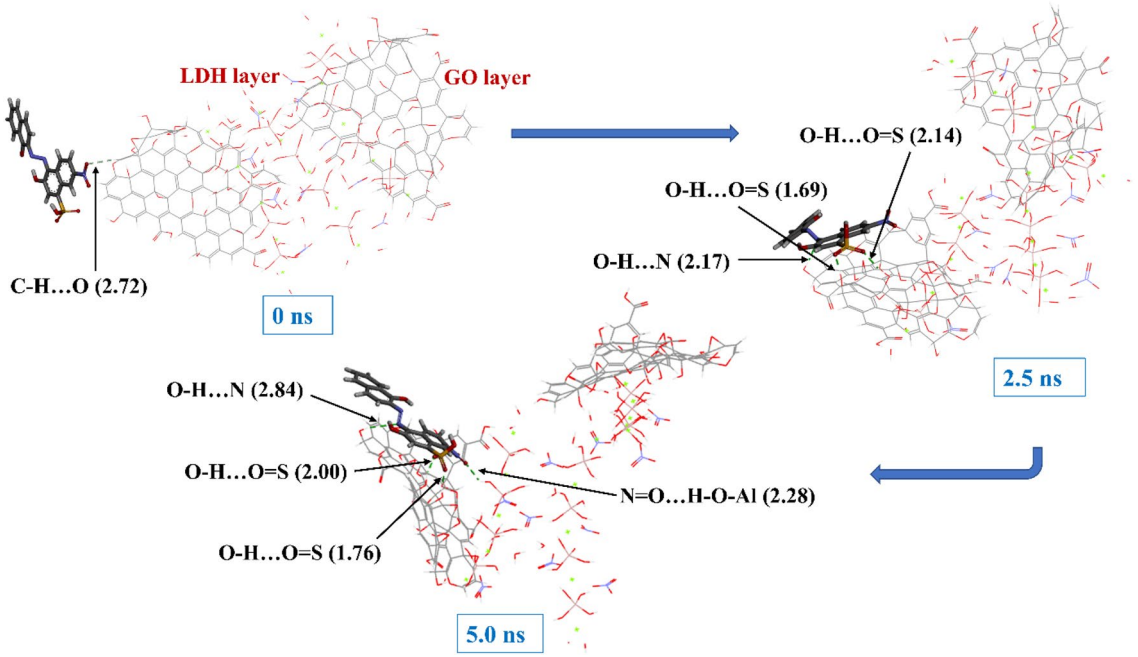

Fig. 5 Simulated adsorption reaction among the LDH-GO and 100 EBT molecules at the low-density condition. Initially (0 ns), the EBT molecule starts interacting with the GO layer using non-classical hydrogen bond (C-H…O). But the EBT molecule is gradually climbing inside of the composite, which means it is going towards LDH layers (2.5 and 5 ns). At 2.5 ns, it interacts with the GO layer only. At 5 ns, it has been seen interacting with LDH layer by N = O…H–O-Al

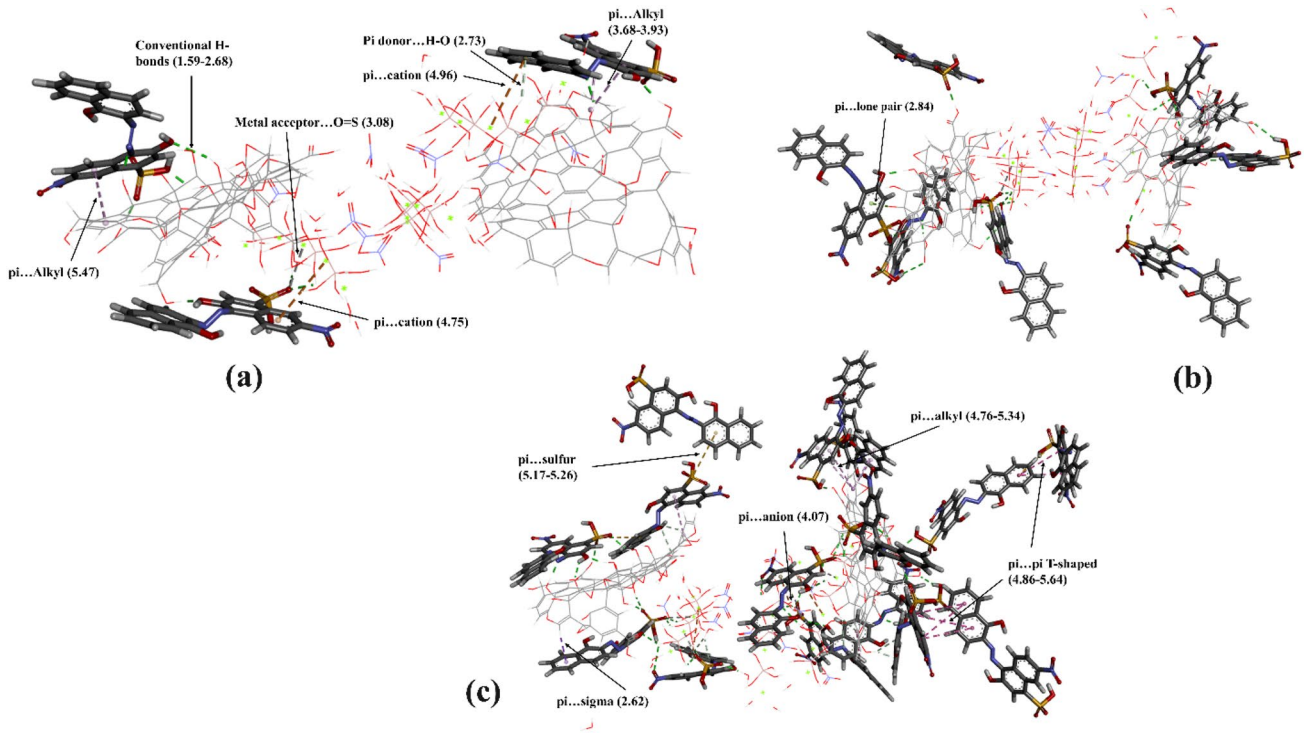

Fig. 6 Simulated adsorption reactions among the LDH-GO composite and 25, 50, and 100 EBT molecules, which are shown by the figures **a**, **b**, and **c**, respectively. At these high-density condition reactions, all possible adsorption sites, nonbonding interaction types, and composite-EBT intermolecular distances have been explored

Attractive forces from π-electrons of the EBT also play important roles in these adsorptions. Since both layers simultaneously participate in the adsorption reaction, delamination of the GO layers on the LDH undoubtedly enhances the adsorption potential of the synthesized composite manifolds compared to the independent GO or LDH materials. These discussions lead to the conclusion that the synthesized LDH-GO composite is stable and efficient to adsorb toxic dye like EBT from low to high concentration solutions.

Conclusions

In this study, the formulated composite material, LDH shielded with GO, was proved as a highly efficient adsorbent to adsorb the anionic Eriochrome Black T molecules compared to the pure LDH material. Both the experimental and molecular dynamics studies proved that the modified material is efficient to adsorb the anionic dye from low to high concentration solutions. Mainly, GO layers helped to improve the adsorption efficacy of the composite by providing new hydrogen bond donor–acceptor atoms and π sites. Anions and cations of the LDH layers also contributed simultaneously by forming interactions with the π-electrons of the EBT molecules.

Supplementary Information The online version contains supplementary material available at https://doi.org/10.1007/s13738-021-02380-z.

Acknowledgements The authors are grateful to Dr. Mohammad A. Halim, CEO of The Red-Green Research Centre, Bangladesh and Assistant professor at the University of Arkansas-Fort Smith, USA for providing the access to use their Gaussian 09 software facility to model the composite.

Declarations

Conflict of interest The authors declare that they have no conflict of interest.

References

1. R. Christie, Environmental aspects of textile dyeing (2007). https://doi.org/10.1533/9781845693091
2. A. Khaleque, D.K. Roy, Removing reactive dyes from textile effluent using banana fibre. Int. J. Basic Appl. Sci. **16**, 14–20 (2016)
3. S. Afshin, Y. Rashtbari, M. Vosoughi, R. Rehman, B. Ramavandi, A. Behzad, L. Mitu, Removal of basic blue-41 dye from water by stabilized magnetic iron nanoparticles on clinoptilolite zeolite. Rev. Chim. **71**(2), 218–229 (2020)
4. G. Samchetshabam, A. Hussan, T.G. Choudhury, Impact of textile dyes waste on aquatic environments and its treatment impact of textile dyes waste on aquatic environments and its treatment. Environ. Ecol. **35**, 2349–2353 (2017)

5. N. Mathur, P. Bhatnagar, P. Nagar, M.K. Bijarnia, Mutagenicity assessment of effluents from textile/dye industries of Sanganer, Jaipur (India): A case study. Ecotoxicol. Environ. Saf. **61**, 105–113 (2005). https://doi.org/10.1016/j.ecoenv.2004.08.003
6. K.R. Mahbub, B. Morium, M.M. Ahmed, M.A. Akond, S. Andrews, Decolourization of novacron blue and novacron super black azo dyes by <I>Bacillus</I> spp isolated from textile effluents in Bangladesh. J. Sci. Res. **7**, 45–53 (2015). https://doi.org/10.3329/jsr.v7i1-2.18682
7. S. Afshin, Y. Rashtbari, M. Shirmardi, M. Vosoughi, A. Hamzehzadeh, Adsorption of basic violet 16 dye from aqueous solution onto mucilaginous seeds of salvia sclarea: kinetics and isotherms studies. Desalin. Water Treat. **161**, 365–375 (2019)
8. R.S. Blackburn, Natural polysaccharides and their interactions with dye molecules: Applications in effluent treatment. Environ. Sci. Technol. (2004). https://doi.org/10.1021/es049972n
9. S. Chakraborty, M.K. Purkait, S. DasGupta, S. De, J.K. Basu, Nanofiltration of textile plant effluent for color removal and reduction in COD. Sep. Purif. Technol. **31**, 141–151 (2003). https://doi.org/10.1016/S1383-5866(02)00177-6
10. Y. Zheng, B. Cheng, J. Fan, J. Yu, W. Ho, Review on nickel-based adsorption materials for Congo red. J. Hazard. Mater. **403**, 123559 (2021). https://doi.org/10.1016/j.jhazmat.2020.123559
11. G. Hatui, G.C. Nayak, G. Udayabhanu, One pot solvothermal synthesis of sandwich-like Mg Al layered double hydroxide anchored Reduced Graphene Oxide: an excellent electrode material for Supercapacitor. Electrochim. Acta. **219**, 214–226 (2016). https://doi.org/10.1016/j.electacta.2016.09.152
12. M.T. Rahman, T. Kameda, T. Miura, S. Kumagai, T. Yoshioka, Application of Mg–Al layered double hydroxide for treating acidic mine wastewater: a novel approach to sludge reduction. Chem. Ecol. **35**, 128–142 (2019). https://doi.org/10.1080/02757540.2018.1534964
13. M.T. Rahman, T. Kameda, S. Kumagai, T. Yoshioka, A novel method to delaminate nitrate-intercalated Mg–Al layered double hydroxides in water and application in heavy metals removal from waste water. Chemosphere **203**, 281–290 (2018). https://doi.org/10.1016/j.chemosphere.2018.03.166
14. F. Li, X. Duan Applications of layered double hydroxides, in: Layer. Double Hydroxides, 1st ed., Springer, Berlin, 2006: pp. 193–223.
15. S. Boubakri, M.A. Djebbi, Z. Bouaziz, P. Namour, N. Jaffrezic-Renault, A.B.H. Amara, M. Trabelsi-Ayadi, I. Ghorbel-Abid, R. Kalfat, Removal of two anionic reactive textile dyes by adsorption into MgAl-layered double hydroxide in aqueous solutions. Environ. Sci. Pollut. Res. **25**, 23817–23832 (2018). https://doi.org/10.1007/s11356-018-2391-6
16. F. Cavani, F. Trifirò, A. Vaccari, Hydrotalcite-type anionic clays: Preparation, properties and applications. Catal. Today. **11**, 173–301 (1991). https://doi.org/10.1016/0920-5861(91)80068-K
17. Q. Wang, D. Ohare, Recent advances in the synthesis and application of layered double hydroxide (LDH) nanosheets. Chem. Rev. **112**, 4124–4155 (2012). https://doi.org/10.1021/cr200434v
18. M.T. Rahman, T. Kameda, S. Kumagai, T. Yoshioka, Effectiveness of Mg–Al-layered double hydroxide for heavy metal removal from mine wastewater and sludge volume reduction. Int. J. Environ. Sci. Technol. **15**, 263–272 (2018). https://doi.org/10.1007/s13762-017-1385-0
19. K. Grover, S. Komarneni, H. Katsuki, Uptake of arsenite by synthetic layered double hydroxides. Water Res. **43**, 3884–3890 (2009). https://doi.org/10.1016/j.watres.2009.06.003
20. T. Kameda, M. Nakamura, T. Yoshioka, Removal of antimonate ions from an aqueous solution by anion exchange with magnesium - Aluminum layered double hydroxide and the formation of a brandholzite-like structure. J. Environ. Sci. Heal-Part A Toxic/Hazardous Subst. Environ. Eng (2012). https://doi.org/10.1080/10934529.2012.668121
21. J. He, M. Wei, B. Li, Y. Kang, D.G. Evans, X. Duan, Preparation of layered double hydroxides, in: Layer. Double Hydroxides, 1st ed., Springer Berlin Heidelberg, Berlin, 2006: pp. 89–119.
22. A.V. Rane, K. Kanny, V.K. Abitha, S. Thomas, Methods for synthesis of nanoparticles and fabrication of nanocomposites. Elsevier (2018). https://doi.org/10.1016/b978-0-08-101975-7.00005-1
23. P. Sivakumar, P.N. Palanisamy, Adsorption studies of Basic Red 29 by a non-conventional activated carbon prepared from Euphorbia antiquorum L. Int. J. ChemTech Res. **1**, 502–510 (2009)
24. G.K. Ramesha, A. Vijaya Kumara, H.B. Muralidhara, S. Sampath, Graphene and graphene oxide as effective adsorbents toward anionic and cationic dyes. J. Colloid Interface Sci. **361**, 270–277 (2011)
25. A.K. Geim, K.S. Novoselov, The rise of grapheme. Nanosci Technol A Collect Rev from Nat Journals (2009). https://doi.org/10.1142/9789814287005_0002
26. S. Park, R.S. Ruoff, Chemical methods for the production of graphenes. Nat. Nanotechnol. **4**, 217–224 (2009). https://doi.org/10.1038/nnano.2009.58
27. D. Li, M.B. Müller, S. Gilje, R.B. Kaner, G.G. Wallace, Processable aqueous dispersions of graphene nanosheets. Nat. Nanotechnol. **3**, 101–105 (2008). https://doi.org/10.1038/nnano.2007.451
28. G.B.B. Varadwaj, O.A. Oyetade, S. Rana, B.S. Martincigh, S.B. Jonnalagadda, V.O. Nyamori, Facile synthesis of three-dimensional Mg-Al layered double hydroxide/partially reduced graphene oxide nanocomposites for the effective removal of Pb2+ from aqueous solution. ACS Appl. Mater. Interfaces. **9**, 17290–17305 (2017). https://doi.org/10.1021/acsami.6b16528
29. J. Bu, L. Yuan, Y. Ren, Y. Lv, Y. Meng, X. Peng, Enhanced removal of eriochrome black T in wastewater by zirconium-based MOF/graphene oxide. Can. J. Chem. **98**, 90–97 (2020). https://doi.org/10.1139/cjc-2019-0368
30. C.R. Minitha, M. Lalitha, Y.L. Jeyachandran, L. Senthilkumar, R.T. Rajendra Kumar, Adsorption behaviour of reduced graphene oxide towards cationic and anionic dyes: Co-action of electrostatic and $\pi - \pi$ interactions. Mater Chem Phys (2017). https://doi.org/10.1016/j.matchemphys.2017.03.048
31. Y.S. Ho, G. McKay, Sorption of dye from aqueous solution by peat. Chem. Eng. J. **70**, 115–124 (1998). https://doi.org/10.1016/S1385-8947(98)00076-X
32. A. Ali, M.S. Rahman, R. Roy, P. Gambill, D.E. Raynie, M.A. Halim, Structure elucidation of menthol-based deep eutectic solvent using experimental and computational techniques. J. Phys. Chem. A. (2021). https://doi.org/10.1021/acs.jpca.0c10735
33. M. Saha, M.S. Rahman, M.N. Hossain, D.E. Raynie, M.A. Halim, M.A. Halim, Molecular and spectroscopic insights of a choline chloride based therapeutic deep eutectic solvent. J. Phys. Chem. A. **124**, 4690–4699 (2020). https://doi.org/10.1021/acs.jpca.0c00851
34. L. Dhar, S. Hossain, M.S. Rahman, S.B. Quraishi, K. Saha, F. Rahman, M.T. Rahman, Adsorption mechanism of methylene blue by graphene oxide shielded Mg-Al layered double hydroxide from synthetic wastewater. J. Phys. Chem. A. **125**, 954–965 (2021). https://doi.org/10.1021/acs.jpca.0c09124
35. S. Weber, N. Modeler, *JCrystalSoft* (California, USA, 2005)
36. D.J. Frisch, M. J.; Trucks, G.W.; Schlegel, H. B.; Scuseria, G. E.; Robb, M. A.; Cheeseman, J. R.; Scalmani, G.; Barone, V.;Mennucci, B.; Petersson, G. A.; Nakatsuji, H.; Caricato, M.; Li, X.; Hratchian, H. P.; Izmaylov, A. F.; Bloino, J.; Zheng, G.; Sonnenber, Gaussian 09 A.02, Gaussian, Inc. Wallingford CT. (2009). 111.
37. M.S. Rahman, S.M. Hossain, M.T. Rahman, M. Kabir, Analysis of iron, scandium, samarium, and zinc in commercial fertilizers and the chemistry behind the stability of these metals in the fertilizers.

J. Agric. Chem. Environ. (2019). https://doi.org/10.4236/jacen.2019.83013
38. S. Kim, P.A. Thiessen, T. Cheng, B. Yu, E.E. Bolton, An update on PUG-REST: RESTful interface for programmatic access to PubChem. Nucleic Acids Res (2018). https://doi.org/10.1093/nar/gky294
39. E. Krieger, R.L. Dunbrack, R.W.W. Hooft, B. Krieger, Assignment of protonation states in proteins and ligands: combining pK a prediction with hydrogen bonding network optimization. Methods Mol. Biol. (2012). https://doi.org/10.1007/978-1-61779-465-0_25
40. E. Krieger, J.E. Nielsen, C.A.E.M. Spronk, G. Vriend, Fast empirical pKa prediction by Ewald summation. J. Mol. Graph. Model. **25**, 481–486 (2006). https://doi.org/10.1016/j.jmgm.2006.02.009
41. E. Krieger, G. Vriend, New ways to boost molecular dynamics simulations. J. Comput. Chem. **36**, 996–1007 (2015). https://doi.org/10.1002/jcc.23899
42. BIOVIADassault Systèmes, Discovery Studio Modeling Environment, in: Dassault Systèmes, San Diego, 2017.